JACS
JOURNAL OF THE AMERICAN CHEMICAL SOCIETY

Article

pubs.acs.org/JACS

Low Temperature Assembly of Functional 3D DNA-PNA-Protein Complexes

Justin D. Flory,[†,‡] Chad R. Simmons,[†,‡,§] Su Lin,[†,§] Trey Johnson,[†,‡] Alessio Andreoni,[†,§] James Zook,[†] Giovanna Ghirlanda,[†,‡] Yan Liu,[†,‡,§] Hao Yan,[†,‡,§] and Petra Fromme*[,†,‡]

[†]Department of Chemistry and Biochemistry, [‡]Center for Bio-Inspired Solar Fuel Production, and [§]Biodesign Institute, Arizona State University, Tempe, Arizona 85287, United States

Supporting Information

ABSTRACT: Proteins have evolved to carry out nearly all the work required of living organisms within complex inter- and intracellular environments. However, systematically investigating the range of interactions experienced by a protein that influence its function remains challenging. DNA nanostructures are emerging as a convenient method to arrange a broad range of guest molecules. However, flexible methods are needed for arranging proteins in more biologically relevant 3D geometries under mild conditions that preserve protein function. Here we demonstrate how peptide nucleic acid (PNA) can be used to control the assembly of cytochrome c (12.5 kDa, pI 10.5) and azurin (13.9 kDa, pI 5.7) proteins into separate 3D DNA nanocages, in a process that maintains protein function. Toehold-mediated DNA strand displacement is introduced as a method to purify PNA-protein conjugates. The PNA-proteins were assembled within 2 min at room temperature and within 4 min at 11 °C, and hybridize with even greater efficiency than PNA conjugated to a short peptide. Gel electrophoresis and steady state and time-resolved fluorescence spectroscopy were used to investigate the effect of protein surface charge on its interaction with the negatively charged DNA nanocage. These data were used to generate a model of the DNA-PNA-protein complexes that show the negatively charged azurin protein repelled away from the DNA nanocage while the positively charged cytochrome c protein remains within and closely interacts with the DNA nanocage. When conjugated to PNA and incorporated into the DNA nanocage, the cytochrome c secondary structure and catalytic activity were maintained, and its redox potential was reduced modestly by 20 mV possibly due to neutralization of some positive surface charges. This work demonstrates a flexible new approach for using 3D nucleic acid (PNA-DNA) nanostructures to control the assembly of functional proteins, and facilitates further investigation of protein interactions as well as engineer more elaborate 3D protein complexes.

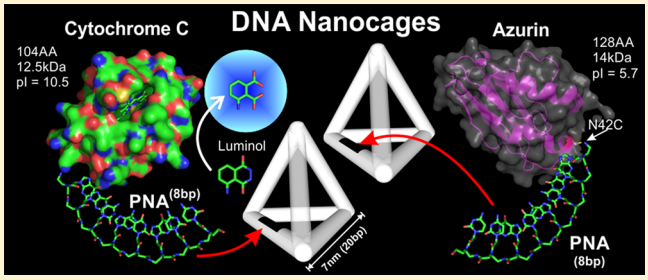

INTRODUCTION

Proteins evolved an enormous diversity of function that is carried out through massively complex pathways of interactions with other biomolecules, which are being compiled into streamlined databases of possible protein−protein interactions and networks.[1,2] However, many of these interactions are dependent on the method used to discover them or are nonfunctional,[3] so new methods are needed to validate and further characterize the specific properties of each interaction.[4] A number of intriguing molecular scaffolds have been developed to arrange proteins, which could be used to study their interactions. Organic ligands can be assembled into nanocages via coordination with metal atoms, which have been used for arranging proteins[5] and other guest molecules.[6] The structures of these organometallic complexes can be solved at high resolution,[7] and used to extract structural information on encapsulated proteins.[5] Coordination cages have been reviewed by Chakrabarty et al.[8] This approach may be more challenging to work with some proteins, because the metals used for building the structures may compete with naturally occurring protein metal centers or modulate the protein structure or activity.[9] Lipid bilayer containing protein nanodiscs[10] can also be assembled, which allow single molecule investigations of membrane proteins in a native-like lipid bilayer[11] and allow study of protein−lipid interactions.[12] *De novo* designed protein−protein interactions have also be used to engineer complex scaffold structures suitable for incorporating guest molecules.[13,14] Protein supercomplexes like ferritin,[15,16] heat shock proteins,[17] and viral capsids[15,18,19] have interior cavities that can be used to encapsulate guest molecules, and have been reviewed by Bode et al.[20] Bacteriophages have also been used to arrange molecules and screen for protein−protein interactions using phage display,[21] which has been reviewed by Sidhu.[22] Protein cages provide atomic level granularity for introducing guest molecules, allow the surface properties to be tuned to promote electrostatic interactions,[23] and facilitate high resolution structure determination.[13,14,24] As molecular scaf-

Received: February 5, 2014
Published: May 14, 2014

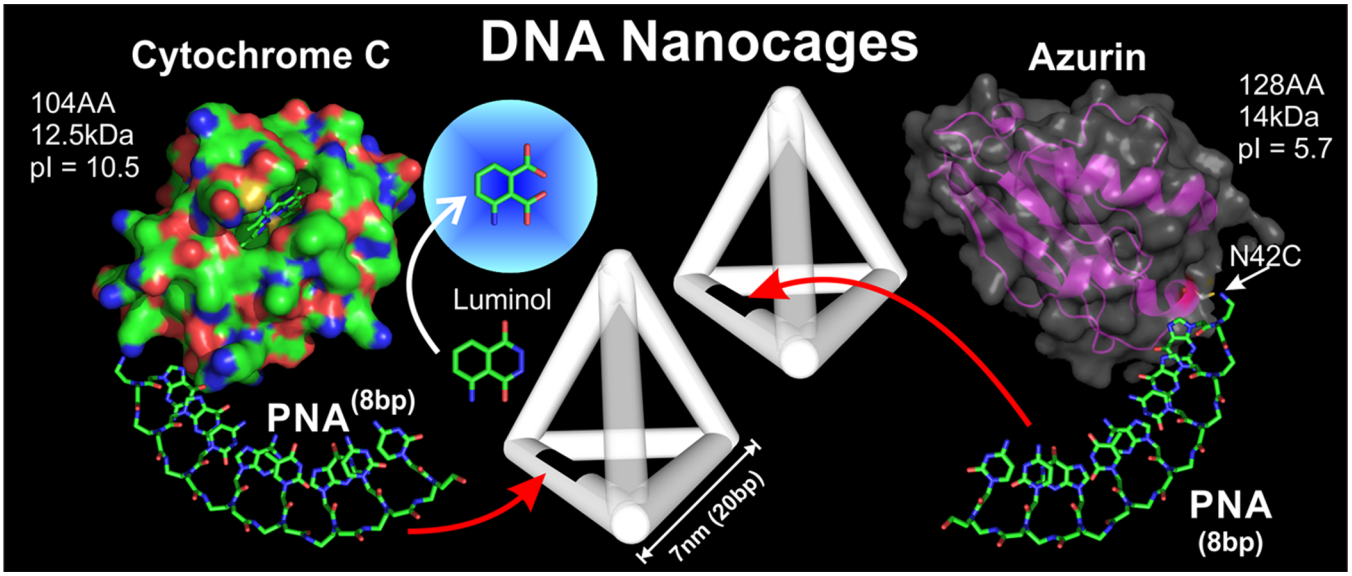

Figure 1. Proposed design to separately assemble two proteins into a DNA nanocage using a PNA linker.

folds for investigating protein−protein interactions, the complex protein surfaces presented in protein cages may be difficult to predict or unravel how the scaffold interacts with the proteins of interest. Furthermore, because the scaffolds are made of protein, they may interfere with surface functionalization chemistry or techniques commonly used to investigate proteins, such as NMR or protein staining.

DNA nanostructures also offer an intriguing platform to study the function of proteins through controlled manipulation of the protein orientation and proximity to other molecules of interest. The field of DNA nanotechnology has been extensively reviewed,[25,26] including specialized reviews focusing on protein functionalization.[27,28] Because these structures are made of DNA they will not interfere with protein specific assays or functionalization methods and present opportunities to access a broader range of molecular tools. The uniform charge density of DNA facilitates simple purification and analysis using ion exchange chromatography or gel electrophoresis under native conditions. The enormous diversity of DNA sequences enables functionalization of large numbers of guest molecules at specific locations driven by complementary base pairing. Furthermore, the surfaces on DNA nanostructures present a more uniform surface compared to proteins, which will simplify decoupling protein−protein interactions from protein−scaffold interactions.

Methods for manipulating proteins on 1D and 2D DNA nanostructures have been utilized for selectively arranging multiple enzymes,[29] investigating DNA binding with aptamers[30] and zinc finger proteins,[31] assembling complementary protein subunits[32] or protein ligands,[33,34] and investigating the spatial dependence of enzyme cascades.[35,36] Three-dimensional DNA nanostructures have been used to encapsulate[37] and arrange proteins[38−40] as well as to organize membrane proteins for NMR structure determination.[41] Because natural protein interactions occur in complex 3D arrangements, there is a need to develop methods for spatially and temporally controlling protein interactions in 3D, which may not be accessible in nanostructures of lower dimension. Furthermore, some proteins contain specific DNA binding domains,[42] and many others are likely influenced by the presence of a negatively charged DNA scaffold, so a better understanding of the electrostatic effects of DNA nanostructures on proteins is needed to establish guidelines for using DNA scaffolds to study proteins. Previous work conjugating protein to DNA has largely focused on introducing proteins onto large 2D DNA lattices[43] or DNA origami nanostructures.[44] Small DNA nanostructures facilitate confining proteins to more biologically relevant interaction distances and frequencies, and can also be more easily incorporated into other materials and complexes.[45] Furthermore, small DNA nanostructures (<100 kDa) allow a higher molar concentration to be achieved, which enables a broader range of protein assays, such as spectroelectrochemistry,[46] and structural analytical techniques, such as circular dichroism,[47] not practical with large DNA origami nanostructures (>4 MDa).[48]

Previously, a DNA tetrahedron was used to encapsulate the protein cytochrome c.[37] In that work the authors directly conjugated the protein to one of the four ssDNAs required for proper assembly of the DNA tetrahedron, and then assembled the DNA−protein complex in a single high temperature annealing step. It is unclear how the protein function was affected by the preparative methods and whether this method could be extended to a wider range of proteins. While it is possible to assemble DNA nanostructures at lower temperature, this generally reduces the assembly yield and complicates purification. Furthermore, if multiple proteins were assembled on the same scaffold in one step, the timing of the interactions could not be controlled. Nucleobase hybridization coupling strategies can overcome this limitation, by first assembling the DNA nanostructure with a binding site for a guest molecule conjugated to a ssDNA, and then incorporating the guest molecule by hybridization under mild conditions.[49,50] However, even oligonucleotides of moderate length can substantially reduce the efficiency of incorporating proteins in close proximity.[50] Peptide nucleic acid (PNA)[51] is an artificial nucleic acid with enhanced binding affinity for DNA that shows great promise for applications in gene targeting[52] and sensing[53,54] and as a nanomaterial.[55−57] We previously showed that 8 nucleotide (nt) strands of PNA can be used to rapidly and efficiently assemble short, fluorescently labeled peptides at room temperature into an existing DNA tetrahedron design[58] modified to include a single-stranded PNA binding domain for

dx.doi.org/10.1021/ja501228c | J. Am. Chem. Soc. 2014, 136, 8283−8295

each peptide.[59] It was unclear if the effectiveness of this strategy could be extended to much longer polypeptides and if it would preserve function.

In this report we conjugate a PNA linker to two small proteins, cytochrome c (12.5 kDa, pI 10.5) and azurin (14 kDa, pI 5.7), and assemble each conjugate into separate 3D DNA nanocages via nucleobase hybridization with the attached PNA linker, as shown in Figure 1. These proteins allowed us to investigate the feasibility of using PNA to assemble longer, functional polypeptides, as well as compare the effect of each protein's net surface charge on its interaction with the negatively charged 3D DNA nanocage. First we synthesized an 8nt PNA sequence and conjugated it to a surface thiol on either protein. Toehold-mediated DNA strand displacement was developed to purify the PNA-protein conjugates from unreacted protein. Gel electrophoresis was used to determine the PNA-protein binding efficiency. Förster resonance energy transfer between the tetramethylrhodamine (TMR) labeled PNA-protein and the fluorescein (FAM) labeled DNA nanocage (DNA-FAM) was used to monitor the PNA-protein hybridization kinetics, thermal dissociation, and separation distances. Time resolved spectroscopy was used to analyze the interaction of the TMR labeled PNA-proteins with the DNA-FAM nanocage. Gel electrophoresis along with steady state and time-resolved fluorescence data were used to construct a model of each DNA-PNA-protein complex. The structure and function of cytochrome c, when conjugated to PNA and hybridized inside the DNA nanocage, was further characterized by measuring the activity of luminol oxidation, determining its redox potential using spectroelectrochemistry, and analyzing its secondary structure using circular dichroism.

RESULTS AND DISCUSSION

DNA-PNA-Protein Complex Design. Previously we demonstrated the PNA-driven assembly of two fluorescently labeled peptides within a DNA nanocage.[59] Briefly, we introduced modifications to an existing DNA tetrahedron design by introducing two 8nt single stranded domains on opposite edges of the DNA nanocage for binding complementary PNA strands with short peptides on the N terminus oriented toward each other through the center of the DNA nanocage. The design allowed the DNA nanocage to be preassembled, purified, and then subsequently populated with one or two PNA-peptides under mild conditions. Here, we extend this strategy to introduce two different metalloproteins into separate DNA nanocages, as shown in Figure 1, at the PNA binding site on one of the edges, as shown in the sequence schematic in Supporting Information Figure S1. Throughout this report we use the nomenclature defined in Supporting Information Figures S1, S2, and S3 when we describe the various strands and constructs used in each experiment.

PNA-Protein Conjugation, Purification, and Fluorescent Labeling. The schemes used to construct conjugates of PNA with either dye labeled or unlabeled azurin or cytochrome c are shown in Figure 2. Detailed methods for the conjugation, purification, and fluorescent labeling can be found in the Supporting Information Measurements and Methods section and discussed further in the Supporting Information Supporting Discussion section. Briefly, the PNA sequence TGCGTGTC-Gly, written from C to N terminus (3′ to 5′), was prepared by microwave-assisted solid phase synthesis as described previously,[59,60] and the free N terminus was labeled

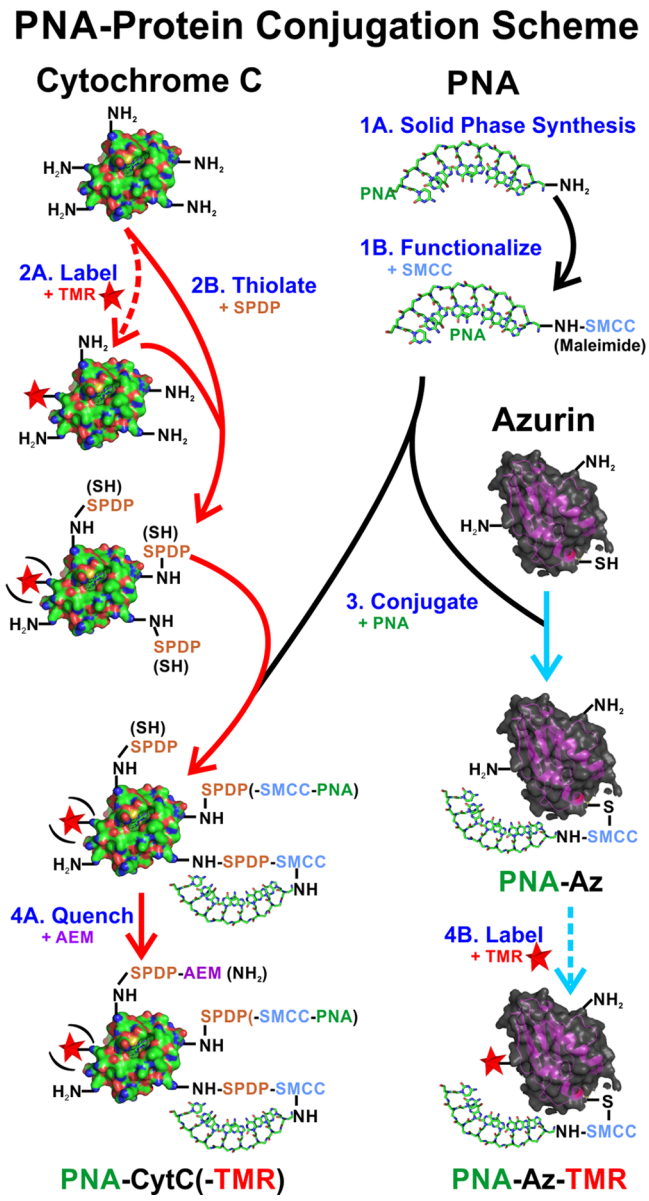

Figure 2. Scheme used to produce the following dye labeled and unlabeled PNA-protein conjugates: PNA-CytC, PNA-CytC-TMR, PNA-Az, PNA-Az-TMR. (1A) Solid phase synthesis of 8nt PNA sequence with N terminal glycine. (1B) Functionalization of PNA with maleimide on N terminus using SMCC cross-linker. (2A) Labeling of cytochrome c surface lysines with TMR dye. (2B) Functionalization of cytochrome c surface lysines with thiols using SPDP cross-linker. (3) Conjugation of PNA-SMCC to surface thiol(s) on cytochrome c and azurin. (4A) Quenching of unreacted surface thiols on cytochrome c with AEM to restore positive charge. (4B) Labeling azurin surface lysines with TMR dye.

with an SMCC cross-linker. PNA-SMCC was conjugated to a single surface cysteine (N42C) containing azurin mutant (~40% yield).[61] The chemical structure of the linker connecting the PNA to azurin is shown in Figure 7B. The SPDP cross-linker was used to introduce 1.1−2.6 thiols per cytochrome c, conjugated to PNA-SMCC (yield 5−10%) and quenched using aminoethylmalemide (AEM) to restore positive surface charges lost during the thiolation of surface amines with SPDP. The chemical structure of the linker connecting the PNA to cytochrome c is shown in Figure 7A.

dx.doi.org/10.1021/ja501228c | J. Am. Chem. Soc. 2014, 136, 8283−8295

Some of the conjugates were dye labeled with TMR for subsequent fluorescent studies.

Further purification of the conjugates was not essential since the remaining free protein could be removed by size exclusion fast protein liquid chromatography (SE-FPLC) after the PNA-protein (15−16 kDa) hybridizes with the much larger DNA nanocage (80 kDa). However, characterization of the PNA-CytC conjugates within a mixture of free protein was challenging due to the low amount of conjugate (5−10%) and the significant absorbance of cytochrome c at 260 nm (ε_{260} = 20 140 M^{-1} cm^{-1}) compared to PNA (ε_{260} = 69 932 M^{-1} cm^{-1}), as shown in Supporting Information Figure S7. Due to the neutral charge and small size of the PNA linker (2.4 kDa) as compared to the protein (12.5 kDa), charge and molecular weight based separation techniques were not effective to separate the PNA-CytC conjugates from unreacted cytochrome c. This motivated our pursuit to develop a new method of purifying PNA-protein conjugates using toehold-mediated DNA strand displacement, as described in the next section.

PNA-Protein Purification by Toehold-Mediated DNA Strand Displacement. In order to further isolate and characterize the PNA-CytC conjugate from the free cytochrome c, we sought to leverage PNAs ability to hybridize to DNA. Toehold-mediated DNA strand displacement is an established technique that uses a partially complementary DNA strand to initially bind a target, but leaves a ssDNA "toehold" domain available for a fully complementary strand to bind and release the target, due to the more favorable binding energies, as reviewed by Zhang and Seelig.[62] Here we adapted this technique to purify PNA-protein conjugates, as shown in Figure 3. To our knowledge this is the first application of this technique for purification purposes. In step 1, the crude mixture of PNA-CytC and free cytochrome c was incubated with either a 16nt or 66nt toehold ssDNA. Each toehold strand contains an 8nt domain (shown in yellow) fully complementary to the 8nt PNA sequence conjugated to the protein, and an 8nt toehold domain (shown in purple) that remains unhybridized. In step 2, the additional mass provided by either the 16nt (4.8 kDa) or 66nt (20.3 kDa) toehold in the DNA-PNA-protein complex allows SE-FPLC to be used to separate it from the free protein. In step 3, a ssDNA fully complementary to the toehold (cDNA) is incubated with the DNA-PNA-protein complex. The cDNA initially binds to the free part of the toehold DNA domain, and then it completely displaces the PNA-protein. In step 4, the cDNA and toehold DNA are removed from the PNA-protein using ion exchange FPLC (IEX-FPLC). The sequences of the strands used in this method are described in Supporting Information Figure S3.

Initially we suspected that the additional charge from the toehold DNA strand would make charge based separation techniques straightforward to isolate the DNA-PNA-protein complexes. Both IEX-FPLC and native PAGE were successful for separating fluorescently labeled PNA strands, as shown in Supporting Information Figures S8 and S9, respectively, which is discussed further in the Supporting Information Supporting Discussion section. Subsequent mixing of the DNA-PNA complex with the fully complementary (cDNA) strand liberated the PNA. When the same method was applied to PNA-CytC, however, the DNA-PNA-CytC hybridization was disrupted during purification. Two major factors may contribute to the dissociation of the toehold DNA from the PNA-CytC: (1) Structural changes to the DNA as it binds to the anion exchange column may weaken its binding to PNA-CytC, and

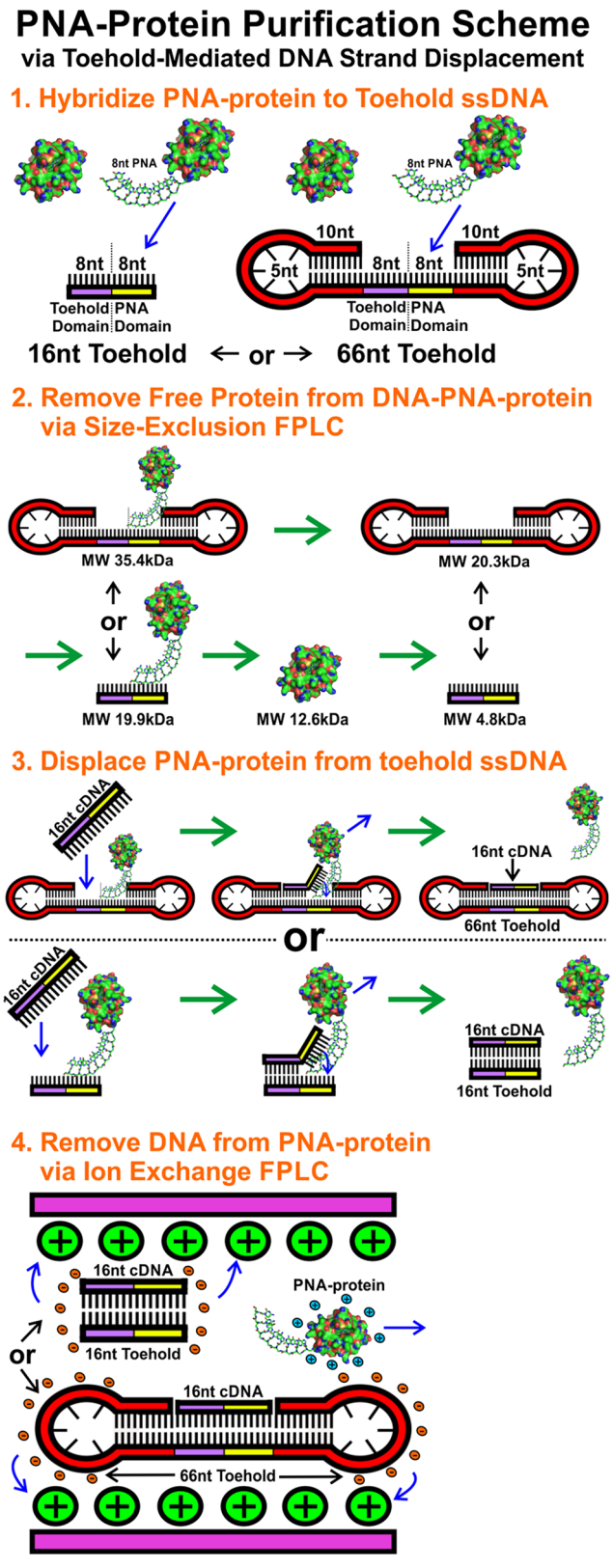

Figure 3. Scheme for purifying PNA-protein using toehold-mediated DNA strand displacement. Details about the procedure are described in the main text.

(2) the dipole moment between the positively charged PNA-CytC and negatively charged DNA may increase the rate of dissociation in the presence of a large electric field during PAGE. To circumvent this issue, we performed SE-FPLC on

dx.doi.org/10.1021/ja501228c | J. Am. Chem. Soc. 2014, 136, 8283−8295

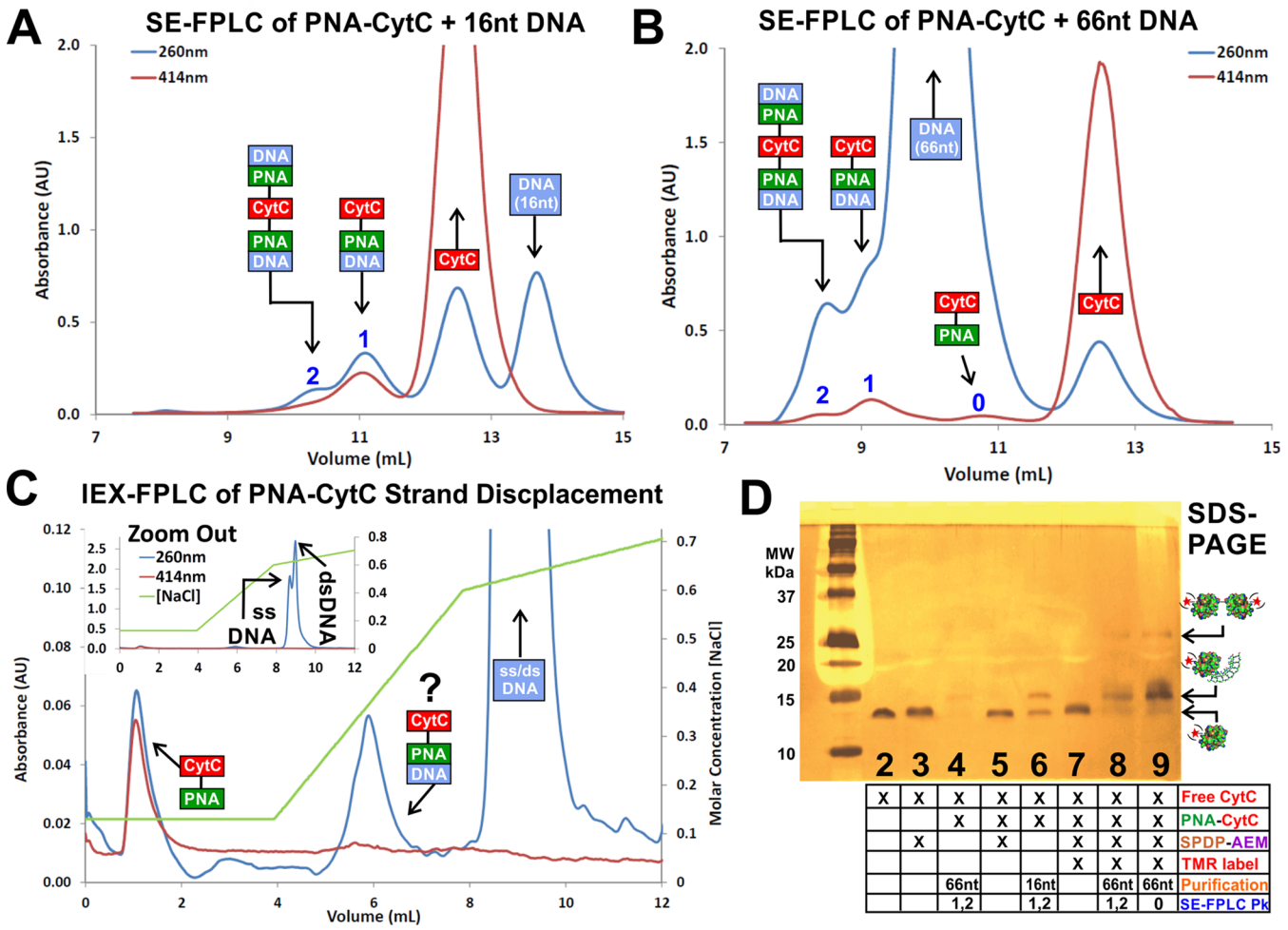

Figure 4. Results for PNA-protein conjugate purification by toehold-mediated strand displacement. Size exclusion (SE) FPLC chromatogram of PNA-CytC (15.1 kDa, ε_{260} = 90k M^{-1} cm^{-1}, ε_{414} = 106k M^{-1} cm^{-1}) incubated with a complementary ssDNA of (A) 16nt (4.8 kDa, ε_{260} = 157k M^{-1} cm^{-1}) and (B) 66nt (20.3 kDa, ε_{260} = 661k M^{-1} cm^{-1}). The nucleobase absorption at 260 nm and heme absorption at 414 nm were monitored to detect the elution of the product. (C) Ion exchange (IEX) FPLC chromatogram showing the toehold and fully complementary ssDNA and corresponding dsDNA retained on the anion exchange column while the cationic PNA-CytC conjugate flows through. (D) Silver stain of a 4% stacking and 15% resolving SDS-PAGE of the SE-FPLC peaks of the PNA-CytC conjugates after purification using different complementary ssDNAs (16nt or 66nt). Lanes 2 and 3 are free cytochrome c and SPDP-AEM modified cytochrome c, respectively (refer to Figure 2 for SPDP-AEM complex); lanes 5 and 7 are the crude PNA-CytC and PNA-CytC-TMR mixtures with free cytochrome c. Lanes 4, 8, and 9 show conjugate purified using the 66nt toehold DNA; lanes 4 and 8 show the overlapping peaks 1 and 2 combined for PNA-CytC and PNA-CytC-TMR, respectively, and lane 9 contains peak 0 from PNA-CytC-TMR.

the DNA-PNA-CytC mixture. Figure 4A shows the SE-FPLC chromatogram with the nucleobase absorbance at 260 nm and the heme absorbance of cytochrome c at 414 nm. Peaks 1 and 2 show significant A_{260} and A_{414}, which we assign to cytochrome c labeled with one (19.7 kDa) and two (26.9 kDa) PNA strands, respectively (masses include complementary toehold DNA strands). We assign the third peak to the free cytochrome c (12.5 kDa), because of the large A_{414} and modest A_{260}. The fourth peak, showing A_{260} but negligible A_{414}, is attributed to unhybridized 16nt toehold DNA strand (4.8 kDa).

In order to improve the separation of the PNA-CytC conjugates, a 66nt (20.3 kDa) toehold strand was designed to induce an even larger mass shift. Figure 4B shows the SE-FPLC chromatogram of PNA-CytC incubated with the 66nt toehold DNA. Peaks 1 and 2 show cytochrome c with one and two PNAs attached, respectively. These peaks show superior separation from the free cytochrome c peak to what was achieved with the 16nt toehold strand. Because of its larger size, the 66nt toehold DNA strand partially overlaps with the PNA-conjugate peaks, but which is removed during the subsequent purification step (vide infra). An additional peak is observed just prior to the free cytochrome c peak (peak 0), which could be PNA-CytC conjugate that dissociated from its complementary toehold DNA during the run.

All PNA-CytC conjugate peaks were collected and then incubated with fully complementary DNA (cDNA) strands to liberate the PNA-CytC conjugate. An IEX-FPLC step was performed to separate the PNA-CytC from the DNA toehold. Figure 4C shows a typical IEX-FPLC chromatogram for the separation: the positively charged PNA-CytC conjugate does not bind to the resin and elutes in the void volume fraction, while the negatively charged ssDNA and dsDNA are retained on the column and are eluted when an increasing salt gradient is applied. The unknown peak eluting before the free DNA may be a small amount of conjugate still bound to the toehold DNA strand that was not completely displaced by the cDNA. Figure 4D shows an SDS-PAGE gel comparing unlabeled and TMR labeled PNA-CytC conjugates after toehold-mediated purifica-

dx.doi.org/10.1021/ja501228c | J. Am. Chem. Soc. 2014, 136, 8283−8295

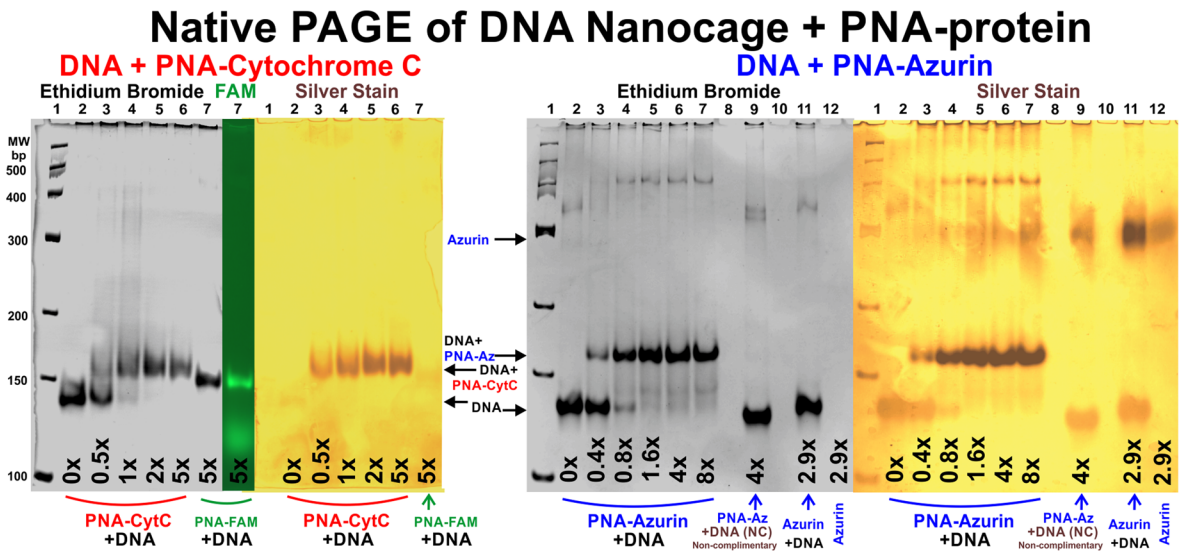

Figure 5. Gel showing the binding of PNA-cytochrome c, PNA-azurin, or PNA-FAM to the DNA nanocage. (Left) Native PAGE (7%), run at 4 °C, of the DNA nanocage incubated with increasing molar excess (0−5×) of PNA-CytC (lanes 2−6) or 5× PNA-FAM (lane 7). From left to right: ethidium bromide staining of all lanes, FAM fluorescence (ex 475 nm, em 535 nm) for lane 7 loaded with PNA-FAM, and silver staining of all lanes. (Right) Native PAGE (7%) of the DNA nanocage incubated with increasing molar excess (0−8×) of PNA-azurin (lanes 2−7), 4× PNA-azurin with a DNA nanocage with a noncomplementary binding sequence (lane 9), 2.9× free azurin with the DNA nanocage (lane 11), and 2.9× free azurin alone (lane 12). From left to right: ethidium bromide and silver staining for all lanes.

tion. On the gel, lanes 2 and 3 were loaded with free cytochrome c and SPDP-AEM modified cytochrome c, respectively (refer to Figure 2 for SPDP-AEM constructs). Both lanes show a single band at the expected molecular weight (~13 kDa). Lanes 5 and 7 were loaded with PNA-CytC and PNA-CytC-TMR, respectively. Both samples were purified by SE-FPLC to remove unreacted PNA, but still contain free cytochrome c. The low fraction of conjugate (~6%) estimated from the UV−vis spectrum was not observed on the gel using silver stain. After toehold-mediated purification of the crude mixtures, the PNA-CytC peak from IEX-FPLC was concentrated and loaded in lane 6. A clear enrichment of the PNA-CytC conjugate is observed when using the 16nt toehold strand. The product obtained using a 66nt toehold DNA to purify PNA-CytC(-TMR) was loaded on lanes 4, 8, and 9. A larger enrichment than what was obtained with the 16nt strand is observed both in the case of PNA-CytC (lane 4) and PNA-CytC-TMR (lanes 8 and 9) conjugates.

PNA-Protein Assembly with the DNA Nanocages. DNA nanocages with an 8nt single stranded domain for binding the PNA-protein conjugates were prepared by thermal annealing as described previously.[59] The DNA nanocage was purified using IEX-FPLC (Supporting Information Figure S10A), as described in the Supporting Information Materials and Methods section and Supporting Discussion section. In separate experiments, the preformed DNA nanocage was incubated at room temperature with increasing molar excess of PNA-CytC, PNA-azurin, or with 5× molar excess of a fluorescently labeled PNA (PNA-FAM).[59] The sample was cooled to 4 °C and then directly analyzed using native PAGE at 4 °C. The results are shown in Figure 5: all the constructs exhibit a band shift upon PNA hybridization to the DNA nanocage. Both PNA-proteins achieve near quantitative binding after stoichiometric amounts are added. This is a noticeable improvement from our previous study of PNA-peptides,[59] which, due to self-aggregation,[63] required 2-fold PNA excess for quantitative binding. This improvement in the hybridization efficiency may be explained by an enhanced solubility of the PNA after conjugation to the protein.

The smallest gel shift, with respect to the empty DNA nanocage, was observed for the binding of PNA-FAM, followed by a slightly larger shift induced from the binding of PNA-CytC, and then a more substantial shift caused from the binding of PNA-azurin. The binding of PNA itself induces a shift as observed previously,[59] likely because the DNA nanocage becomes more rigid as the single stranded binding domain for PNA becomes double stranded. The slight additional shift observed for PNA-CytC is likely due to a lower overall negative charge of the DNA-PNA-CytC nanocage assembly after binding the positively charged cytochrome c (pI ~10.5). The substantial shift induced by PNA-azurin suggests that the negatively charged protein is repelled away from the DNA nanocage; this increases the hydrodynamic radius of the assembly, therefore causing a slower migration in the gel, as compared with the empty DNA nanocage. A substantial gel shift was also observed for the same DNA nanocage attached to a slightly larger but also negatively charged green fluorescent protein (28 kDa, pI 5.7)[39] as well as streptavidin.[40] An alternative "inverted" DNA nanocage design was assembled that moved the PNA binding domain across the helix, rotating the orientation of the point of protein attachment by about 180° (sequences described in Supporting Information Figure S1). After incubating PNA-Az-TMR with the original DNA nanocage design as well as the inverted DNA nanocage design (DNAi), native PAGE showed no difference in the mobility of the complexes, as shown in Supporting Information Figure S10C lanes 2−5. A possible explanation for this is that, regardless of the orientation provided by the PNA attached to the DNA nanocage, the glycine-SMCC linker provides sufficient flexibility for the protein to adopt its most thermodynamically favored orientation, on the basis of the surrounding environment. The gel for azurin also shows that PNA-Az does not bind to the DNA nanocage with a noncomplementary sequence (lane 9) and free azurin does

dx.doi.org/10.1021/ja501228c | J. Am. Chem. Soc. 2014, 136, 8283−8295

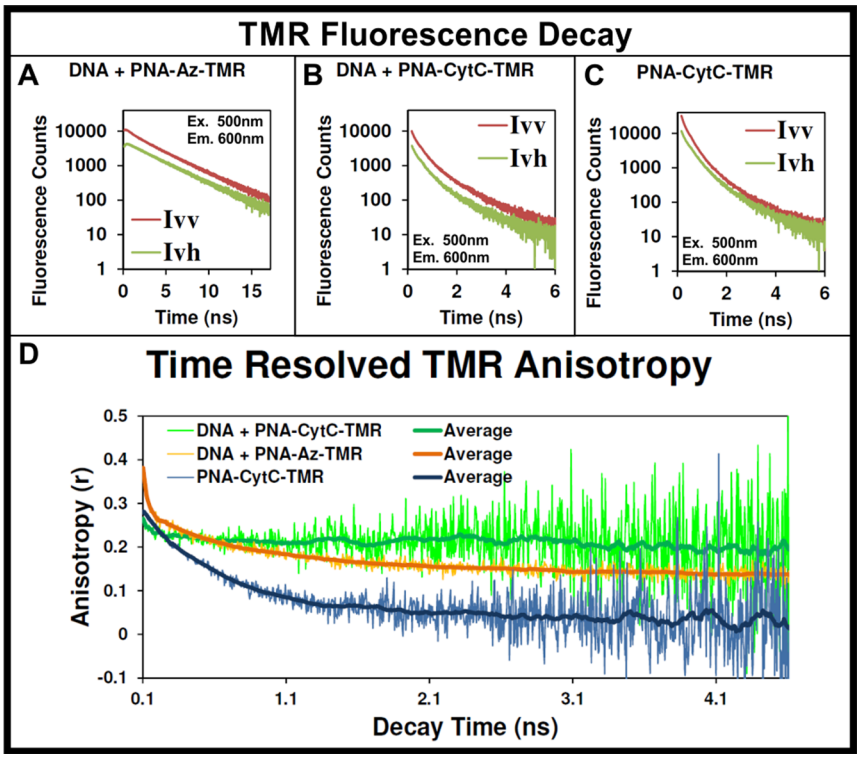

Figure 6. Fluorescence decay and anisotropy of two TMR dye labeled proteins hybridized to a DNA nanocage with PNA. (A, B, C) Plot of the parallel (Ivv) and perpendicular (Ivh) TMR fluorescence decay of PNA-Az-TMR hybridized to the DNA nanocage (A), and of PNA-CytC-TMR when hybridized to the DNA nanocage (B) and when free in solution (C). (D) The anisotropy for each data point of the decays, shown in panels A, B, and C, was calculated as described in the Supporting Information Materials and Methods section, and the results are plotted here. The central moving average for each data set is reported in the same plot for clarity.

not bind to the DNA nanocage (lane 11). Similar results were obtained for controls using PNA-CytC, as shown in Supporting Information Figure S11, demonstrating the PNA strand is required to properly assemble the protein into the DNA nanocage. The silver stain also shows the negatively charged free azurin and unbound PNA-Az migrate as a single band at ~300bp, which is reasonable given a 70% lower charge density than the DNA nanocage.

The kinetics of PNA-protein hybridization into the DNA nanocage was investigated at room temperature by monitoring quenching of the FAM labeled DNA nanocage fluorescence emission as TMR labeled PNA-proteins were added, as discussed in the Supporting Information Supporting Discussion section. PNA-Az-TMR and PNA-CytC-TMR were found to reach 99% hybridization within 2 min, as shown in Supporting Information Figure S12. These rates are faster than the 5−10 min previously observed for TMR labeled PNA-peptides.[59] PNA-CytC-TMR was also found to hybridize to the DNA nanocage within 4 min at 11 °C. Since proteins are normally kept frozen or chilled to extend their useful lifetime, hybridization at low temperature may be ideal to study temperature sensitive proteins or protein complexes. The cytochrome c heme absorbance was also found to quench FAM fluorescence upon binding to the DNA nanocage. Unlabeled PNA-CytC hybridized within 13 min at 25 °C and within 25 min at 11 °C, suggesting that the TMR dye label may facilitate binding of PNA-CytC. TMR is known to interact with DNA nucleobases, which may help to keep the protein close to the DNA nanocage to facilitate PNA hybridization.[64] The dissociation temperature (T_D) of the TMR labeled PNA-proteins bound to the FAM labeled DNA nanocage was determined by monitoring FRET of the complex while the temperature was slowly increased from 11 to 85 °C, as shown in Supporting Information Figure S13. The measured T_D of both PNA-proteins were 3−4 °C lower than the theoretical value for the PNA sequence alone. This indicates that the presence of either protein destabilizes the PNA-DNA duplex to the same degree.

Fluorescence Characterization: Anisotropy, Lifetime, and Energy Transfer. The arrangement of both proteins in the DNA nanocage environment was further investigated using fluorescence spectroscopy. We used time-correlated single photon counting (TCSPC) to evaluate how freely the dye labels can rotate when attached to the PNA-protein and when hybridized into the DNA nanocage by probing the rate of depolarization of their emission when excited by polarized light. Each complex was excited by vertically polarized light at 500 nm, and the emission of TMR was monitored at 600 nm with polarization both parallel (VV, vertical excitation and emission) and perpendicular (VH, vertical excitation and horizontal emission) relative to the polarization of the excitation, as shown in Figure 6 (A−C). The difference in the emission intensity of VV and VH was used to calculate the anisotropy decay kinetics using the equations described in the Supporting Information Materials and Methods section. The anisotropy decay and corresponding central moving average are plotted for each complex as a function of time in Figure 6D. The maximum possible anisotropy value is 0.4 for a perfectly rigid complex with no depolarization, whereas the minimum value of zero indicates a rapidly rotating dye molecule that has fully depolarized. The anisotropy for TMR decays with three distinct components, a <0.2 ns fast component due to energy

dx.doi.org/10.1021/ja501228c | J. Am. Chem. Soc. 2014, 136, 8283−8295

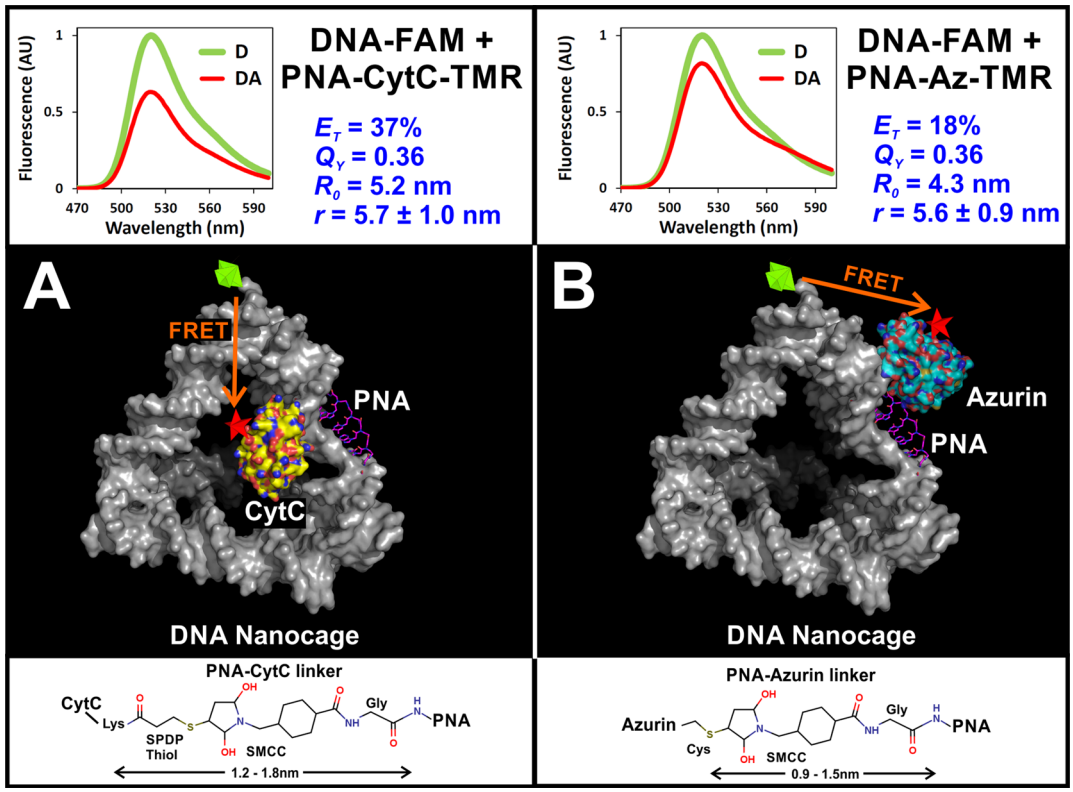

Figure 7. Steady state fluorescence spectra, molecular model of the DNA-PNA-protein complexes, and linker chemical structure. (Top) Fluorescence emission spectra (ex 450 nm) of the donor only (D) and of the donor with the acceptor (DA) measured at 11 °C of the DNA-FAM nanocage with PNA-CytC-TMR (A) or PNA-Az-TMR (B). Each spectra also shows the calculated energy transfer efficiency (E_T), the determined quantum yield (Q_Y), calculated Förster radius (R_0), and Förster distance (r). (Middle) Molecular models of the dye labeled DNA nanocage hybridized to either a dye labeled PNA-cytochrome c conjugate (A) or PNA-azurin conjugate (B), with an arrow indicating the direction of energy transfer. The chemical structure of the linkers used to conjugate PNA to each protein is shown below each model.

transfer between proteins with multiple TMR labels, a 0.2−2 ns intermediate component due to the rotation of the protein, and a >2 ns slow component due to the rotation of the DNA nanocage. Interpretation of the anisotropy decay of the fast components and absolute anisotropy values of the slow components are complex due to the differences in TMR labeling of both proteins and are discussed further in the Supporting Information Supporting Discussion section. The intermediate decay component (0.2−2 ns) due to protein rotation is observed for PNA-Az-TMR in the DNA nanocage and for PNA-CytC-TMR in solution but not for PNA-CytC-TMR in the DNA nanocage. This suggests that cytochrome c remains within and closely interacts with the DNA nanocage, which significantly restricts its rotation, while azurin is repelled away from the DNA nanocage and rotates quite freely.

Additional TCSPC measurements were performed to obtain information on the position of each of the proteins inside the DNA nanocage after hybridization. The fluorescence emission decay of FAM on an empty DNA-FAM nanocage was compared to the decay of the same label after either PNA-CytC-TMR or PNA-Az-TMR were hybridized to the DNA-FAM nanocage. The results of these experiments are shown in Supporting Information Figure S15. From the time dependent intensity decay it is clear that the lifetime of FAM is reduced upon binding of either of the two TMR-labeled PNA-protein conjugates. The average lifetimes determined from fitting the data in Supporting Information Figure S15 with exponential functions are presented in Supporting Information Table S2. The change in FAM lifetime in the presence of each TMR-labeled PNA-protein was used to determine the energy transfer efficiency of 17 ± 5% for PNA-Az-TMR and 37 ± 3% for PNA-CytC-TMR as described in the Supporting Information Materials and Methods section. The fluorescence decay kinetics of a DNA nanocage labeled with FAM at the vertex adjacent to the TMR labeled PNA-protein was also measured at various wavelengths between 500 and 640 nm that span the FAM emission spectrum. The data were fit using a global analysis algorithm and plotted as a function of wavelength in the decay associated spectra (DAS) shown in Supporting Information Figure S16. Both the DAS and fluorescence decay indicate that energy transfer occurs from FAM to TMR in the DNA-PNA-protein nanostructures. These data are furthered discussed in the Supporting Information Supporting Discussion section.

Together with TCSPC, steady state fluorescence spectroscopy was used to measure the distance between the TMR labeled PNA-proteins and the DNA nanocage vertex labeled with FAM. The steady state fluorescence spectra of DNA-FAM + PNA-CytC-TMR and DNA-FAM + PNA-Az-TMR were recorded at 11 °C, and are shown in Figure 7A,B, respectively. Figure 7 reports the following for each construct: the fluorescence spectra of the donor (D), the fluorescence spectra of the donor in the presence of the acceptor (DA), the energy transfer efficiency (E_T), the quantum yield of FAM bound to DNA (Q_Y), the Förster radius of the FAM-TMR FRET pair (R_0), and the Förster distance in the construct (r). The values of E_T, Q_Y, R_0, and r were calculated as described by Flory et al.[59] The energy transfer efficiency values calculated from the intensity change of the DNA-FAM fluorescence in the presence

dx.doi.org/10.1021/ja501228c | J. Am. Chem. Soc. 2014, 136, 8283−8295

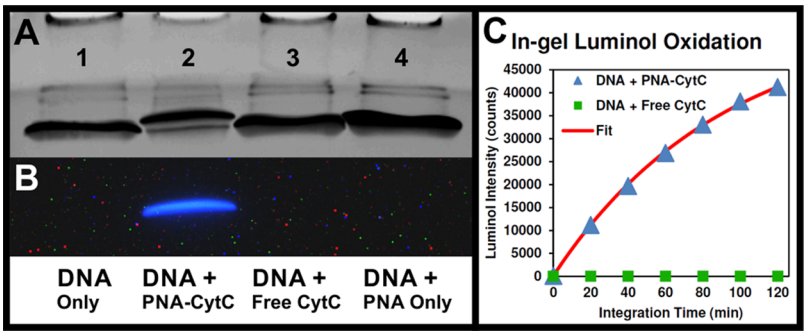

Figure 8. In-gel activity of PNA-cytochrome c bound to the DNA nanocage. (A) Ethidium bromide stain of a 4% stacking and 15% resolving native PAGE of 100 pmols of DNA nanocage alone (lane 1), DNA + PNA-CytC (lane 2), the DNA nanocage incubated with 5× free cytochrome c (lane 3) and separately incubated with 5× PNA-FAM (lane 4). (B) Chemiluminescence image of the gel from part A due to luminol oxidation by PNA-CytC in the DNA nanocage. (C) Integrated chemiluminescence band intensities of DNA-PNA-CytC and DNA + free CytC taken every 20 min.

of either PNA-CytC-TMR or PNA-Az-TMR were 37% and 18%, respectively. These values agree well with the 37 ± 3% and 17 ± 5% calculated using the change in DNA-FAM lifetime as measured by TCSPC. The Förster radii for the FRET pairs DNA-FAM with PNA-CytC-TMR-FAM or PNA-Az-TMR were calculated to be 5.2 and 4.3 nm, respectively. The larger Förster radius for PNA-CytC-TMR was due to the greater overlap of its absorption spectrum with the DNA-FAM emission spectrum. The details of the calculations, as well as discussion about the spectral data used to obtain these values, are presented in the Supporting Information Measurements and Methods section. The Förster distances separating the FAM label on the DNA nanocage from the PNA-CytC-TMR or PNA-Az-TMR were found to be 5.7 ± 1.0 nm and 5.6 ± 0.9 nm, respectively.

With the constraint that both proteins have approximately the same separation distance from the adjacent DNA nanocage vertex, we developed a model of the DNA-PNA-protein complexes that accounts for differences observed during PAGE and time-resolved anisotropy, as shown in Figure 7. The significantly larger PAGE gel shift and faster anisotropy decay kinetics observed for TMR labeled PNA-azurin attached to the DNA nanocage suggest it is repelled away from the DNA nanocage creating a larger hydrodynamic radius for the complex and allows the protein to rotate freely. PNA-CytC induces a gel shift similar to that observed for the PNA alone, suggesting that the protein is confined within the DNA nanocage. The TMR anisotropy decay due to PNA-CytC rotation in solution is absent when hybridized into the DNA nanocage suggesting that PNA-CytC is tightly interacting with the DNA nanocage, and thus restricts its rotation. The chemical linkers used to connect PNA to each protein are shown in Figure 7 along with the projected length. Our model suggests that, despite the same PNA binding site in the DNA nanocage, these chemical linkers are not rigid enough to hold two similarly sized proteins at the same location. Instead, the flexibility of the linker allows each protein to find a favorable orientation based on its surface electrostatic interactions with the negatively charged DNA nanocage. To improve control over the protein in the future, it may be advantageous to operate near the isoelectric point of the protein, increase the salt concentration, add a second specific conjugation site to further constrain the orientation of the protein, or include a complementary protein in an adjacent part of the DNA nanocage that can form a stable protein−protein complex.

Cytochrome c Activity. One of the most challenging aspects of working with proteins is to identify relevant *in situ* methods to assess the integrity of their structural and functional properties. Cytochrome c is a redox active heme containing protein that functions as an electron carrier in the mitochondrion. Like other heme containing proteins, such as horseradish peroxidase, it has the ability to oxidize luminol in the presence of hydrogen peroxide to produce chemiluminescence. Furthermore, the heme absorbance at 550 nm changes significantly upon oxidation and reduction, thereby facilitating the spectroscopic assessment of its oxidation state. Wild type azurin is a copper containing redox active protein; however, the mutant used in this study contained redox inactive zinc in the metal center.

The activity of cytochrome c in the DNA-PNA-CytC complex was analyzed directly in a native polyacrylamide gel using the luminol assay, where the gel was imaged for 2 h to monitor the progression of the reaction, as described in the Supporting Information Materials and Methods section. Figure 8A,B shows the ethidium bromide stain and luminol chemiluminescence, respectively, of the DNA nanocage alone (lane 1), the DNA nanonocage with PNA-CytC (lane 2), the DNA nanocage incubated with 5× free cytochrome c (lane 3) and separately incubated with 5× PNA-FAM (lane 4). All DNA constructs migrate uniformly, with a noticeable shift for the DNA-PNA-CytC containing band from the empty DNA nanocages. Only the DNA-PNA-CytC complex shows chemiluminescence. The intensity of the DNA-PNA-CytC (lane 2) and DNA + free cytochrome c (lane 3) bands in each image was integrated and plotted as a function of integration time, as shown in Figure 8C. Cytochrome c demonstrates substrate diffusion-limited kinetic behavior as it catalyzes the oxidation of luminol in the DNA nanocage, which is in agreement with what was observed in solution.[65]

Cytochrome c Redox Potential. The redox potential of cytochrome c was also investigated inside the DNA nanocage by monitoring the ratio of oxidized and reduced cytochrome c based on the absorbance change at 550 nm. The potential of the solution was adjusted using the ferricyanide−ferrocyanide redox couple, as described in the Supporting Information Materials and Methods section. A schematic of the reaction is shown in Figure 9A. The fraction of ferricytochrome c (oxidized) is plotted as a function of the heme absorption spectra in Figure 9B. The log of the ratio of ferrocytochrome c to ferricytochrome c is plotted against the log of the ratio of ferrocyanide to ferricyanide (which set the solution potential)

dx.doi.org/10.1021/ja501228c | J. Am. Chem. Soc. 2014, 136, 8283−8295

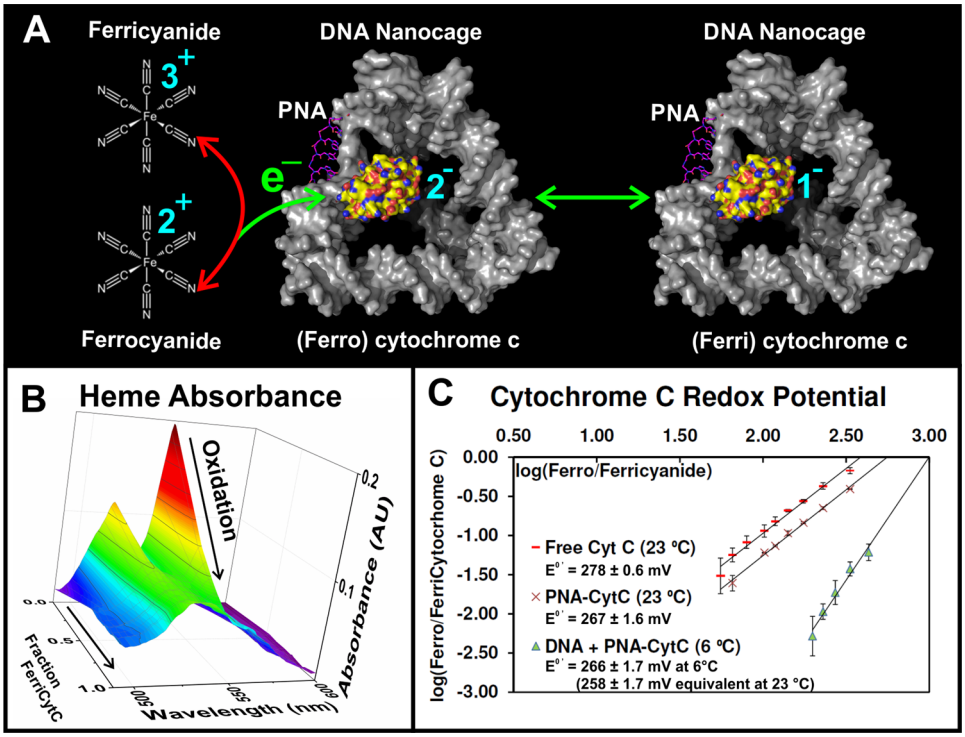

Figure 9. Spectroelectrochemical results of PNA-cytochrome when bound to the DNA nanocage. (A) Schematic of the oxidation of ferrocytochrome to ferricytochrome c inside the DNA nanocage by ferricyanide. (B) Absorption spectra of the DNA-PNA-CytC complex as a function of the fraction of ferricytochrome c (oxidized). (C) Log of the ratio of ferrocytochrome c to ferricytochrome c plotted against the log of the ratio of ferrocyanide to ferricyanide for free cytochrome c (red) and DNA-PNA-CytC (green). Also shown is a linear fit of each data set and the calculated redox potential values.

as shown in Figure 9C. The *x* intercept of a linear fit of this plot determines the potential at equilibrium between ferri- and ferrocytochrome c, which can be used to determine the redox potential using the Nernst equation. The calculated potential for free horse heart cytochrome c was 278 ± 0.6 mV at 23 °C, which is about 10 mV higher than reported elsewhere,[66] and may be due to a systematic offset in our experimental setup. The calculated redox potential for PNA-CytC in solution was found to be 267 ± 1.6 mV at 23 °C. The experiment for the DNA-PNA-CytC complex was carried out at 6 °C to ensure the PNA-CytC stayed hybridized to the DNA nanocage. The redox potential of cytochrome c is known to be inversely dependent on temperature (−0.45 mV/°C), which has been explained due to the higher ordering of water at low temperature stabilizing the cytochrome c conformation in the reduced state.[67,68] The calculated redox potential for PNA-CytC when incorporated into the DNA nanocage was found to be 266 ± 1.7 mV at 6 °C with an equivalent potential of 258 ± 1.7 mV at 23 °C.

The 10 mV negative shift in the cytochrome c redox potential observed after conjugation to PNA and additional 10 mV shift observed once PNA-CytC is incorporated into the DNA nanocage may both be due to a less positive net charge of the protein, which helps to stabilize the net positive charge of the heme in the oxidized state. The positive charges from some surface lysine residues are displaced during PNA conjugation. Furthermore, close interaction of cytochrome c with the negatively charged DNA nanocage may neutralize some positive surface charges on the protein. This shows a similar trend to that reported for ferrocene conjugated to ssDNA upon hybridization with a complementary ssDNA.[69,70] The DNA microenvironment was also shown to effect the activity of a *β*-lactamase enzyme attached to a giant *λ* DNA (48.5 kbp) strand when the DNA was toggled between an unfolded and compact state.[71] This suggests that PNA and DNA nanostructures may be able to modulate the activity of proteins through a variety of mechanisms. Together, the activity and redox potential data indicate that the preparation of the PNA-CytC conjugates as well as the incorporation of the conjugates in a DNA nanocage maintain functionality of the protein.

Cytochrome c Secondary Structure. Circular dichroism (CD) of cytochrome c was used to determine the effect of conjugating PNA and hybridizing into the DNA nanocage on the secondary structure of the protein, as described in the Supporting Information Measurements and Methods section. The UV CD spectrum of cytochrome c and PNA-CytC (Supporting Information Figure S17A) both show similar negative-in-sign peaks at 222 and 208 nm and a positive-in-sign peak at 195 nm in agreement with the literature,[72] suggesting that the overall secondary structure of cytochrome c is unaffected by PNA conjugation. CD of the Soret band has also been used as a structural probe of the bond strength of the axial Met(80) ligand to the heme iron in the oxidized state of cytochrome c.[73] A pronounced negative-in-sign peak at 417 nm occurs in the oxidized state when Met(80) is in close proximity to the heme iron, but which disappears upon denaturation. The Soret CD spectra of cytochrome c, PNA-CytC, and DNA-PNA-CytC (Supporting Information Figure S17B) all show a negative-in-sign peak at 417 nm suggesting cytochrome c retains its native conformation around the heme active site after conjugation with PNA and incorporation into the DNA nanocage. This is further supported by nearly identical heme absorption spectra in both the oxidized and reduced states, as shown in Supporting Information Figure S18.

dx.doi.org/10.1021/ja501228c | J. Am. Chem. Soc. 2014, 136, 8283−8295

CONCLUSION

We have demonstrated gentle methods to conjugate, purify, and assemble protein into a 3D DNA nanocage using a PNA linker. The results obtained with cytochrome c suggest that the methodology preserves protein structure and function. Toehold-mediated DNA strand displacement is introduced as an effective method for purifying PNA and enriching PNA-protein conjugates. Each of the PNA-protein conjugates was assembled into separate DNA nanocages within 2 min at room temperature, and within 4 min at 11 °C. The presence of protein increased the PNA solubility, allowing the PNA-protein conjugate to bind to the DNA nanocage in near stoichiometric quantities, with faster binding kinetics and with increased hybridization efficiency than the same PNA sequence conjugated to a short, neutral peptide.[59] The effect of the surface charge of two different proteins on their interactions with a DNA nanocage was also investigated. Gel electrophoresis and steady state and time-resolved fluorescence spectroscopy data were used to propose a model of the DNA-PNA-protein complexes. Our model suggests that the negatively charged azurin is repelled away from the DNA nanocage, whereas the positively charged cytochrome c remains within and closely interacts with the DNA nanocage. When incorporated into the DNA nanocage, cytochrome c maintained catalytic activity and secondary structure, and its redox potential was reduced modestly by 20 mV possibly due to neutralization of positive surface charges during PNA conjugation and from close interaction with the DNA nanocage.

This report describes a flexible approach to studying protein function and interactions within a 3D nucleic acid framework. The design could be further expanded to connect up to 4−6 polypeptides (up to 60 kDa)[37] on adjacent edges of the DNA nanocage by introducing the appropriate PNA binding sequences. The ability to systematically introduce different proteins into defined locations within such a three-dimensional structure may facilitate investigations of protein−protein interactions. The maturation of the DNA nanotechnology field has greatly simplified the process of designing a wide variety of DNA nanostructures. Our method of incorporating proteins into 3D DNA nanostructures by means of a PNA linker facilitates exploiting the enormous diversity of DNA nanostructures for investigating and engineering functional 3D protein-nucleic acid complexes.

ASSOCIATED CONTENT

Supporting Information

Materials and Methods section and calculations for the TMR spectra and extinction coefficients, hybridization kinetics, PAGE band integration, redox potential, and anisotropy. Supporting Discussion section detailing the PNA-protein conjugate purification, PNA purification via toehold-mediated DNA strand displacement, DNA nanocage purification by IEX-FPLC, kinetics of PNA-protein hybridization into DNA nanocage, TMR absorption spectra and anisotropy of PNA-protein conjugates, fluorescence decay kinetics of DNA-FAM + PNA-protein-TMR. Figure S1 containing DNA and PNA sequences and schematic showing their arrangement in the complex. Figure S2 showing complex nomenclature with list of required DNA and PNA-protein strands for assembly. Figure S3 containing DNA sequences for toehold-mediated PNA purification. Figure S4 containing MALDI-MS spectrum and RP-HPLC of PNA-Gly-SMCC. Figure S5 showing MALDI-MS spectrum and SDS-PAGE of azurin conjugated to PNA-SMCC. Figure S6 showing quantification of SPDP thiolation of cytochrome c by MALDI-MS and UV−vis. Figure S7 containing MALDI-MS spectrum of SPDP thiolated cytochrome c conjugated to PNA-SMCC. Figure S8 containing native PAGE (7%) at 4 °C of toehold-mediated ssDNA purification of PNA. Figure S9 showing IEX-FPLC of toehold-mediated ssDNA purification of PNA. Figure S10 showing DNA nanocage assembly and PNA incubation. Figure S11 containing native PAGE (7%) at 4 °C of the DNA nanocage incubated with PNA-CytC. Figure S12 showing time course PNA-protein hybridization with the DNA nanocage. Figure S13 containing fluorescence spectra of the TMR labeled PNA-proteins bound to the FAM labeled DNA nanocage as a function of temperature. Figure S14 containing calculated dye labeled PNA-protein absorption spectra and spectral changes upon hybridization to the DNA nanocage. Figure S15 showing donor (FAM) fluorescence decay kinetics attached to DNA nanocage with and without the acceptor (TMR) labeled PNA-proteins hybridized to the DNA nanocage. Figure S16 showing decay associated spectra (DAS) of the FAM labeled DNA nanocage hybridized to either the TMR labeled PNA-azurin or PNA-cytochrome c. Figure S17 containing circular dichroism of cytochrome c, PNA-CytC, and DNA-PNA-CytC. Figure S18 containing visible spectra of cytochrome c, PNA-CytC, and DNA-PNA-CytC. Table S1 detailing fitting parameters and time to reach 99% hybridization for PNA-protein binding kinetics with DNA nanocage. Table S2 detailing lifetime components and calculated average lifetimes of the donor and acceptor fluorophores. This material is available free of charge via the Internet at http://pubs.acs.org.

AUTHOR INFORMATION

Corresponding Author

Petra.Fromme@asu.edu.

Author Contributions

The authors declare no competing financial interests.

Notes

The authors declare no competing financial interest.

ACKNOWLEDGMENTS

We want to thank Professor Dr. Gerard Canters for his support of Dr. Alessio Andreoni during the preparation of azurin, Dayn Sommers for consultation on spectroscopic redox titration, John Lopez for sharing his expertise on CD, Associate Professor Dr. Kevin Redding for use of the B0631081 cuvette, Jay-How Yang and Dr. Jose M. Martin-Garcia for consultation on SDS-PAGE, and J. Domingo Meza-Aguilar for consultation on SE-FPLC of PNA-CytC. This work was supported by the Center for Bio-Inspired Solar Fuel Production, an Energy Frontier Research Center funded by the U.S. Department of Energy, Office of Science, Office of Basic Energy Sciences, under Award DE-SC0001016.

REFERENCES

(1) Franceschini, A.; Szklarczyk, D.; Frankild, S.; Kuhn, M.; Simonovic, M.; Roth, A.; Lin, J.; Minguez, P.; Bork, P.; von Mering, C.; Jensen, L. J. *Nucleic Acids Res.* **2013**, *41*, D808−15.

(2) Chatr-Aryamontri, A.; Breitkreutz, B.-J.; Heinicke, S.; Boucher, L.; Winter, A.; Stark, C.; Nixon, J.; Ramage, L.; Kolas, N.; O'Donnell, L.; Reguly, T.; Breitkreutz, A.; Sellam, A.; Chen, D.; Chang, C.; Rust,

J.; Livstone, M.; Oughtred, R.; Dolinski, K.; Tyers, M. *Nucleic Acids Res.* **2013**, *41*, D816−23.
(3) Wodak, S. J.; Vlasblom, J.; Turinsky, A. L.; Pu, S. *Curr. Opin. Struct. Biol.* **2013**, *23*, 941−953.
(4) Mosca, R.; Pons, T.; Céol, A.; Valencia, A.; Aloy, P. *Curr. Opin. Struct. Biol.* **2013**, *23*, 929−940.
(5) Fujita, D.; Suzuki, K.; Sato, S.; Yagi-Utsumi, M.; Yamaguchi, Y.; Mizuno, N.; Kumasaka, T.; Takata, M.; Noda, M.; Uchiyama, S.; Kato, K.; Fujita, M. *Nat. Commun.* **2012**, *3*, 1093.
(6) Chakrabarty, R.; Stang, P. J. *J. Am. Chem. Soc.* **2012**, *134*, 14738−14741.
(7) Sun, Q.-F.; Iwasa, J.; Ogawa, D.; Ishido, Y.; Sato, S.; Ozeki, T.; Sei, Y.; Yamaguchi, K.; Fujita, M. *Science* **2010**, *328*, 1144−1147.
(8) Chakrabarty, R.; Mukherjee, P. S.; Stang, P. J. *Chem. Rev.* **2011**, *111*, 6810−6918.
(9) Gaetke, L. *Toxicology* **2003**, *189*, 147−163.
(10) Bayburt, T. H.; Sligar, S. G. *FEBS Lett.* **2010**, *584*, 1721−1727.
(11) Nath, A.; Trexler, A. J.; Koo, P.; Miranker, A. D.; Atkins, W. M.; Rhoades, E. *Single-Molecule Fluorescence Spectroscopy Using Phospholipid Bilayer Nanodiscs*, 1st ed.; Elsevier Inc.: New York, 2010; Vol. *472*, pp 89−117.
(12) Kijac, A.; Shih, A. Y.; Nieuwkoop, A. J.; Schulten, K.; Sligar, S. G.; Rienstra, C. M. *Biochemistry* **2010**, *49*, 9190−9198.
(13) King, N. P.; Sheffler, W.; Sawaya, M. R.; Vollmar, B. S.; Sumida, J. P.; Andre, I.; Gonen, T.; Yeates, T. O.; Baker, D.; André, I.; Gonen, T.; Yeates, T. O.; Baker, D. *Science* **2012**, *336*, 1171−1174.
(14) Lai, Y.-T.; Cascio, D.; Yeates, T. O. *Science* **2012**, *336*, 1129.
(15) Douglas, T.; Dickson, D. P.; Betteridge, S.; Charnock, J.; Garner, C. D.; Mann, S. *Science* **1995**, *269*, 54−57.
(16) Ueno, T.; Suzuki, M.; Goto, T.; Matsumoto, T.; Nagayama, K.; Watanabe, Y. *Angew. Chem.* **2004**, *116*, 2581−2584.
(17) Abedin, M. J.; Liepold, L.; Suci, P.; Young, M.; Douglas, T. *J. Am. Chem. Soc.* **2009**, *131*, 4346−4354.
(18) Comellas-Aragonès, M.; Engelkamp, H.; Claessen, V. I.; Sommerdijk, N. A. J. M.; Rowan, A. E.; Christianen, P. C. M.; Maan, J. C.; Verduin, B. J. M.; Cornelissen, J. J. L. M.; Nolte, R. J. M. *Nat. Nanotechnol.* **2007**, *2*, 635−639.
(19) Minten, I. J.; Hendriks, L. J. A.; Nolte, R. J. M.; Cornelissen, J. J. L. M. *J. Am. Chem. Soc.* **2009**, *131*, 17771−17773.
(20) Bode, S. A.; Minten, I. J.; Nolte, R. J. M.; Cornelissen, J. J. L. M. *Nanoscale* **2011**, *3*, 2376−2389.
(21) Koide, A.; Gilbreth, R. N.; Esaki, K.; Tereshko, V.; Koide, S. *Proc. Natl. Acad. Sci. U.S.A.* **2007**, *104*, 6632−6637.
(22) Sidhu, S. S.; Koide, S. *Curr. Opin. Struct. Biol.* **2007**, *17*, 481−487.
(23) Wörsdörfer, B.; Woycechowsky, K. J.; Hilvert, D. *Science* **2011**, *331*, 589−592.
(24) Uchida, M.; Klem, M. T.; Allen, M.; Suci, P.; Flenniken, M.; Gillitzer, E.; Varpness, Z.; Liepold, L. O.; Young, M.; Douglas, T. *Adv. Mater.* **2007**, *19*, 1025−1042.
(25) Pinheiro, A. V.; Han, D.; Shih, W. M.; Yan, H. *Nat. Nanotechnol.* **2011**, *6*, 763−772.
(26) Linko, V.; Dietz, H. *Curr. Opin. Biotechnol.* **2013**, *24*, 555−561.
(27) Saccà, B.; Niemeyer, C. M. *Chem. Soc. Rev.* **2011**, *40*, 5910−5921.
(28) Diezmann, F.; Seitz, O. *Chem. Soc. Rev.* **2011**, *40*, 5789−5801.
(29) Numajiri, K.; Yamazaki, T.; Kimura, M.; Kuzuya, A.; Komiyama, M. *J. Am. Chem. Soc.* **2010**, *132*, 9937−9939.
(30) Zhou, C.; Yang, Z.; Liu, D. *J. Am. Chem. Soc.* **2012**, *134*, 1416−1418.
(31) Nakata, E.; Liew, F. F.; Uwatoko, C.; Kiyonaka, S.; Mori, Y.; Katsuda, Y.; Endo, M.; Sugiyama, H.; Morii, T. *Angew. Chem.* **2012**, *124*, 2471−2474.
(32) Erkelenz, M.; Kuo, C.-H.; Niemeyer, C. M. *J. Am. Chem. Soc.* **2011**, *133*, 16111−16118.
(33) Englund, E. A.; Wang, D.; Fujigaki, H.; Sakai, H.; Micklitsch, C. M.; Ghirlando, R.; Martin-Manso, G.; Pendrak, M. L.; Roberts, D. D.; Durell, S. R.; Appella, D. H. *Nat. Commun.* **2012**, *3*, 614.
(34) Eberhard, H.; Diezmann, F.; Seitz, O. *Angew. Chem., Int. Ed.* **2011**, *50*, 4146−4150.
(35) Wilner, O. I.; Weizmann, Y.; Gill, R.; Lioubashevski, O.; Freeman, R.; Willner, I. *Nat. Nanotechnol.* **2009**, *4*, 249−254.
(36) Fu, Y.; Zeng, D.; Chao, J.; Jin, Y.; Zhang, Z.; Liu, H.; Li, D.; Ma, H.; Huang, Q.; Gothelf, K. V.; Fan, C. *J. Am. Chem. Soc.* **2013**, *135*, 696−702.
(37) Erben, C. M.; Goodman, R. P.; Turberfield, A. J. *Angew. Chem., Int. Ed.* **2006**, *118*, 7574−7577.
(38) Zhang, C.; Tian, C.; Guo, F.; Liu, Z.; Jiang, W.; Mao, C. *Angew. Chem., Int. Ed.* **2012**, *51*, 3382−3385.
(39) Duckworth, B. P.; Chen, Y.; Wollack, J. W.; Sham, Y.; Mueller, J. D.; Taton, T. A.; Distefano, M. D. *Angew. Chem.* **2007**, *119*, 8975−8978.
(40) Wong, N. Y.; Zhang, C.; Tan, L. H.; Lu, Y. *Small* **2011**, *7*, 1427−1430.
(41) Douglas, S.; Chou, J.; Shih, W. *Proc. Natl. Acad. Sci. U.S.A.* **2007**, *104*, 6644−6648.
(42) Wolfe, S.; Nekludova, L.; Pabo, C. *Annu. Rev. Biophys. Biomol. Struct.* **2000**, *29*, 183−212.
(43) Yan, H.; Park, S. H.; Finkelstein, G.; Reif, J. H.; LaBean, T. H. *Science* **2003**, *301*, 1882−1884.
(44) Saccà, B.; Meyer, R.; Erkelenz, M.; Kiko, K.; Arndt, A.; Schroeder, H.; Rabe, K. S.; Niemeyer, C. M. *Angew. Chem., Int. Ed.* **2010**, *49*, 9378−9383.
(45) Simmons, C. R.; Schmitt, D.; Wei, X.; Han, D.; Volosin, A. M.; Ladd, D. M.; Seo, D.-K.; Liu, Y.; Yan, H. *ACS Nano* **2011**, *5*, 6060−6068.
(46) Myer, Y.; Saturno, A.; Verma, B.; Pande, A. *J. Biol. Chem.* **1979**, *254*, 11202−11207.
(47) Greenfield, N. *Nat. Protoc.* **2007**, *1*, 2876−2890.
(48) Rothemund, P. W. K. *Nature* **2006**, *440*, 297−302.
(49) Pal, S.; Deng, Z.; Ding, B.; Yan, H.; Liu, Y. *Angew. Chem., Int. Ed.* **2010**, *122*, 2760−2764.
(50) Fu, J.; Liu, M.; Liu, Y. *J. Am. Chem. Soc.* **2012**, *22*, 5516−5519.
(51) Nielsen, P. E.; Egholm, M.; Berg, R. H.; Buchardt, O. *Science* **1991**, *254*, 1497−1500.
(52) Onyshchenko, M. I.; Gaynutdinov, T. I.; Englund, E. A.; Appella, D. H.; Neumann, R. D.; Panyutin, I. G. *Nucleic Acids Res.* **2011**, *39*, 7114−7123.
(53) Pokorski, J. K.; Nam, J. M.; Vega, R. A.; Mirkin, C. A.; Appella, D. H. *Chem. Commun.* **2005**, 2101−2103.
(54) Liu, J.; Cao, Z.; Lu, Y. *Chem. Rev.* **2009**, *109*, 1948−1998.
(55) Lytton-Jean, A. K. R.; Gibbs-Davis, J. M.; Long, H.; Schatz, G. C.; Mirkin, C. A.; Nguyen, S. T. *Adv. Mater.* **2009**, *21*, 706−709.
(56) Lukeman, P. S.; Mittal, A. C.; Seeman, N. C. *Chem. Commun.* **2004**, 1694−1695.
(57) Gaillard, C.; Girard, H. a.; Falck, C.; Paget, V.; Simic, V.; Ugolin, N.; Bergonzo, P.; Chevillard, S.; Arnault, J. C. *RSC Adv.* **2014**, *4*, 3566.
(58) Goodman, R. P.; Schaap, I. A. T.; Tardin, C. F.; Erben, C. M.; Berry, R. M.; Schmidt, C. F.; Turberfield, A. J. *Science* **2005**, *310*, 1661−1665.
(59) Flory, J. D.; Shinde, S.; Lin, S.; Liu, Y.; Yan, H.; Ghirlanda, G.; Fromme, P. *J. Am. Chem. Soc.* **2013**, *135*, 6985−6993.
(60) Fabani, M. M.; Abreu-Goodger, C.; Williams, D.; Lyons, P. A.; Torres, A. G.; Smith, K. G. C.; Enright, A. J.; Gait, M. J.; Vigorito, E. *Nucleic Acids Res.* **2010**, *38*, 4466−4475.
(61) Van Amsterdam, I. M. C.; Ubbink, M.; Einsle, O.; Messerschmidt, A.; Merli, A.; Cavazzini, D.; Rossi, G. L.; Canters, G. W. *Nat. Struct. Biol.* **2001**, *9*, 48−52.
(62) Zhang, D. Y.; Seelig, G. *Nat. Chem.* **2011**, *3*, 103−113.
(63) Sahu, B.; Sacui, I.; Rapireddy, S.; Zanotti, K. J.; Bahal, R.; Armitage, B. A.; Ly, D. H. *J. Org. Chem.* **2011**, *76*, 5614−5627.
(64) Wang, L.; Gaigalas, A. K.; Blasic, J.; Holden, M. J. *Spectrochim. Acta, Part A* **2004**, *60*, 2741−2750.
(65) Radi, R.; Thomson, L.; Rubbo, H.; Prodanov, E. *Arch. Biochem. Biophys.* **1991**, *288*, 112−117.
(66) Wallace, C. J.; Proudfoot, A. E. *Biochem. J.* **1987**, *245*, 773−779.

(67) Anderson, C.; Halsall, H. *Biochem. Biophys. Res. Commun.* **1977**, *76*, 339−344.
(68) Taniguchi, I.; Iseki, M.; Eto, T. *Bioelectrochem. Bioenerg.* **1984**, *174*, 373−383.
(69) Hansen, M. N.; Farjami, E.; Kristiansen, M.; Clima, L.; Pedersen, S. U.; Daasbjerg, K.; Ferapontova, E. E.; Gothelf, K. V. *J. Org. Chem.* **2010**, *75*, 2474−2481.
(70) Ihara, T.; Maruo, Y.; Takenaka, S.; Takagi, M. *Nucleic Acids Res.* **1996**, *24*, 4273−4280.
(71) Rudiuk, S.; Venancio-Marques, A.; Baigl, D. *Angew. Chem., Int. Ed.* **2012**, *51*, 12694−12698.
(72) Myer, Y. *J. Biol. Chem.* **1968**, *243*, 2115−2122.
(73) Santucci, R.; Ascoli, F. *J. Inorg. Biochem.* **1997**, *68*, 211−214.